Geopersia 2022, 12(1): 69-87
DOI: 10.22059/GEOPE.2021.325668.648622

RESEARCH PAPER

# Implication of well logs for evaluation of a carbonate reservoir: an example, the Sarvak Formation, Zagros Basin, SW Iran

**Moosa Esfandyari, Hassan Mohseni ***

Department of Geology, Faculty of Sciences, Bu-Ali Sina University, Hamedan Iran

Received: 16 June 2021, Revised: 24 July 2021, Accepted: 13 August 2021


**Abstract**
Petrophysical evaluation of well log data of the Mid Cretaceous rocks (Upper part of the Sarvak Formation) were conducted for the Marun oil field. Rock and fluid volumetric indices, such as porosity type and distribution, water saturation, and lithology, were estimated from density, resistivity, neutron porosity, sonic and gamma ray logs. Petrophysical parameters including shale volume ($V_{sh}$), total porosity (PHT), effective porosity (PHE), water saturation (Sw), hydrocarbon saturation ($S_h$) and lithology were calculated. Matrix Identification (MID), M-N, NPHI- RHOB, NPHI- DT cross-plots indicated that the Sarvak Formation is mainly composed of carbonate lithology. Results also indicated that shale volume varies between 0.1% and 23.3%; total and effective porosities are between 0.8% and 47.2% and between 0.1% and 45.1%, respectively. Various primary and secondary porosities do exist in the Sarvak Formation. Majority of the porosities are preferentially developed in the middle part of this oil field. Water saturation is between 2% and 100%. The results reveal that the reservoir characterization of the Sarvak Formation is very variable and fluctuating from poor to good reservoir units. Apparently, $S_w$ increases toward the center of the reservoir and eastward as well. This is probably in part controlled by fractures that are preferentially concentrated in the middle part of the anticline.

**Keywords:** Petrophysical Parameters, Formation Evaluation, Well Log Analysis, Reservoir Geology, Water Saturation.

## Introduction

Identification of reservoir rocks and evaluation of their quality is important and necessary for hydrocarbon exploitation. Hence, to perform precise and accurate evaluation of reservoir rocks, appropriate geologic and petrophysical information is necessary (Selley, 1998). Among various procedures, interpretation of well log data is the most important task to estimate and quantifying some of the most important reservoir characteristics such as porosity, water saturation and finally the pay zones (Schlumberger, 1974; Rider, 2002; Sarasty and Stewart, 2003; Abd El-Gawad, 2007; Mostafa & Walid, 2003; Sharma et al., 2020). Integrating different geophysical data allows to estimate physical properties in the subsurface and reducing the ambiguities of the interpretation (Wu & Grana, 2017).

The aim of petrophysical studies is to evaluate the reservoir quality in different parts of a formation, reservoir zoning to determine the most suitable zones for the optimal reservoir exploitation and more conscious development of an oil field. Proper estimation of petrophysical parameters plays an effective role in reservoir modelling and simulation, and the degree of success of many exploration, drilling and exploitation activities of hydrocarbon reservoirs depends on the accuracy of estimating these parameters. The principal goal of reservoir

* Corresponding author e-mail: mohseni@basu.ac.ir

characterization is to outsmart nature to obtain more recoveries with fewer wells in better positions with minimum cost (Haldorsen & Damsleth, 1993).

Reservoir parameters and data are determined by two common methods: direct core analysis and/or evaluation of well data. Core analysis is very expensive and time- consuming, and also the limitation of that cores are not normally available for all of the boreholes. But well logs are commonly available for most of the wells which provide a plenty of petrophysical dada. Petrophysical evaluation of well log data has always been crucial for identification and assessment of hydrocarbon bearing zones (Kumar et al., 2017; Ellis, 2008).

In this research, the reservoir quality in terms of petrophysical parameters like shale volume, effective porosity, water and hydrocarbon saturations, were examined in the Mid Cretaceous Sarvak Formation in Marun oilfield (SW Iran). In order to attain more accuracy, a 3-D model was constructed to give a better understanding of spatial distribution of these parameters. The results of this study could improve the understanding of the relationship between petrophysical properties and the hydrocarbon system of the oilfield. In other words, the forthcoming studies could focus on those sectors of the reservoir that have the greatest potential for hydrocarbon production (upper Sarvak).

## Geological setting

The Middle East oil province, has been well appreciated by petroleum geologists due the numerous oil and gas reserves. The petroleum system, including source rocks, reservoirs, and effective cap rocks at appropriate time horizons, has made the region very important (Al Sharhan, & Narin, 2003). Thick sedimentary successions of Cretaceous age in the Arabian Plate and the Zagros Basin contain numerous economically important hydrocarbon accumulations (Ghabeishavi et al., 2010; Hollis, 2011; Lapponi, 2011). The Zagros Basin predominantly comprises thick intervals of carbonates, siliciclastics and subordinate evaporitic horizons. These successions are characterized by a marked reduction in siliciclastic influx, the development of a carbonate platform surrounded by intra-shelf basin, and deposition of basinal source rocks. Sediments of the Sarvak Fm. were deposited on platform and within the intrashelf basin on the passive margin on the Arabian Plate (Ziegler, 2001). The stratigraphic record of the Late Albian, Cenomanian and Turonian (89-98.9 Ma) in the Arabian Plate and the Zagros Basin includes the Mishrif, Ahmadi and Rumaila Formations in Saudi Arabia; the Natih Formation in Oman (Van Buchem et al., 2002); the Mishrif Formation in Iraq; and the Sarvak Formation in Iran. This formation (Albian - Turonian) contains more than 20% oil-in-place of Iranian oil reserves in the SW of Iran, serving as the second most important oil reservoir after the Asmari Formation (Bordenave & Hegre, 2010). The Marun oil field is located in the Dezful Embayment (a subdivision of the Zagros basin), (Fig. 1). The Sarvak Formation in the type section (Bangestan anticline) overlies the Kazhdumi Formation and unconformably underlies the Gurpi Formation, although in most parts of the basin, especially in the Dezful Embayment, the upper boundary is associated with deposition of the Ilam Formation (James and Wynd, 1965; Beiranvand et al. 2007; Rahimpour-Bonab et al. 2012) (Fig. 2). The Sarvak Formation comprises two principal facies: a massive limestone deposited in a shallow-water platform, composed of rudists, other bivalves, gastropods, diverse benthic foraminifera, and a deep-marine thin-bedded facies, composed of small oligostegenids and planktonic fauna (James & Wynd 1965). The combination of the effects of eustatic sea-level falls, tectonic movements, local salt diapirism, and the rejuvenation of basement faults resulted in the formation of some local and regional disconformities in the Cenomanian–Turonian succession (Rahimpour-Bonab et al. 2013). These surfaces and the related processes have had major effects on the reservoir characteristics of the Sarvak Formation (Taghavi et al. 2007; Hajikazemi et al. 2010; Hollis 2011; Rahimpour-Bonab et al. 2013).

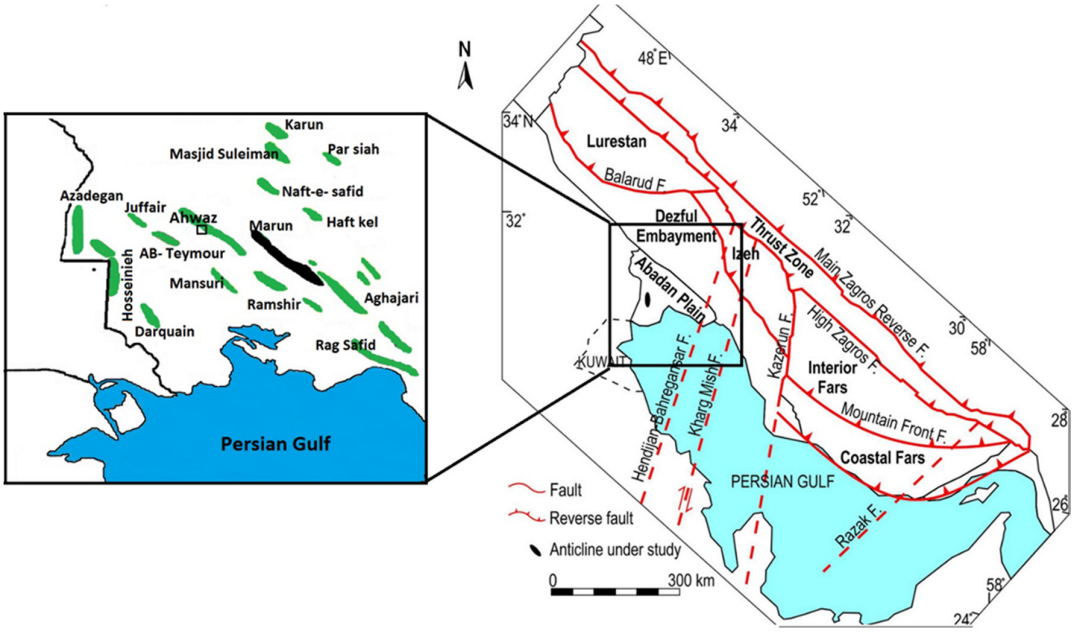


**Figure 1.** Location map of the studied oil field in the Zagros basin (after Moradi et al., 2017)

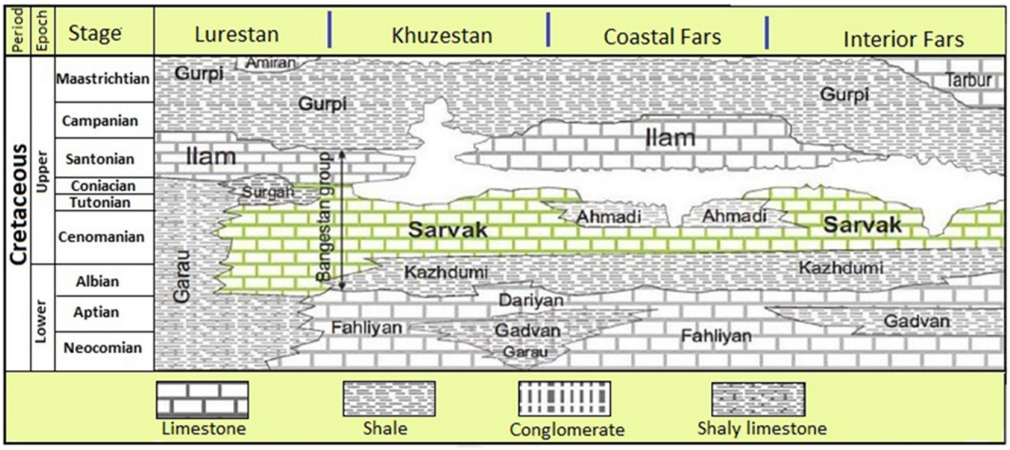


**Figure 2.** The Cretaceous stratigraphic chart of the Zagros and the position Sarvak Formation (modified from Rahimpour-Bonab et al., 2012)

The complex tectonic history of the Zagros Basin and Arabian Plate led to vigorous variations in reservoir characteristics of the Sarvak Formation and the lateral equivalent intervals (Alavi, 2004; Sepehr and Cosgrove, 2004; Casini et al., 2011; Rahimpour- Bonab et al., 2012), which brought the formation of intrashelf basins and paleo-highs in the SW sector of the Zagros basin (including the Dezful Embayment). The microfacies, depositional environment and reservoir framework of the Sarvak Formation has been well described in the Zagros and Persian Gulf basins (e.g., Setudehnia 1978; Taghavi et al. 2006; Razin et al. 2010; Sharp et al. 2010; van Buchem et al. 2011; Rahimpour- Bonab et al. 2012, 2013; Vincent et al. 2015). Despite its importance, few studies addressed the potential implication of well log data for petrophysical evaluation, particularly where less direct sources of data (i.e. core samples) are available.

## Materials and methods

Thin sections of cutting chips and core samples were examined to determine microfacies and interpret the depositional setting. Petrophysical analyses were performed based on well logs

including shallow and deep resistivity logs (LLD, ILS and MSFL), neutron porosity (NPHI), bulk density (RHOB), acoustic travel time (DT) and gamma ray (CGR), which were collected from selected wells (9 wells) using Geolog 7.1®. Lithology of different strata were determined by using resistivity, density or gamma-ray log (Schlumberge, 1991; 2009). Lithological and mineralogical composition of the reservoir were also identified based on Schlumberge (2009) charts (i.e. neutron vs. density, neutron vs. gamma ray, neutron-sonic, M–N and Matrix Identification (MID) cross plots). M-N plots were used to achieve the lithology-dependent parameters, and were calculated based on using eqs. 1 and 2).

$$M= [(\Delta T_f- \Delta T_{log})/ (\rho_b- \rho_f)]. 0.01 \quad (1)$$

$$N= (\emptyset_{Nf}- \emptyset_N)/ (\rho_b- \rho_f) \quad (2)$$

where $\Delta t_f$, is the interval transit time in the fluid within the formation [for fresh water; 189 (μsec/ft); for salt water; 185 (μsec/ft)], $\Delta t_{log}$, is the interval transit time in the formation in μsec/ft, $\rho_b$ is the bulk density and $\rho_f$ is the mud filtrate density, $\emptyset_{Nf}$ and $\emptyset_N$ is the fluid neutron porosity and formation neutron porosity respectively.

The shale volume ($V_{sh}$) was calculated from CGR log using equation 3 (Tiab, 2000).

$$V_{Sh}= (CGR_{log}- CGR_{min})/ (CGR_{max}- CGR_{min}) \quad (3)$$

where $V_{sh}$ is the volume of shale; $CGR_{log}$ stands for CGR log reading; $CGR_{max}$ and $CGR_{min}$ represent maximum and minimum CGR log readings of the adjacent strata respectively.

The porosities were estimated using a combination of the density and neutron logs.

$$\emptyset_D= (\rho_{ma}- \rho_b)/ (\rho_{ma}- \rho_f) \quad (4)$$

where $\emptyset_D$, $\rho_b$, $\rho_{ma}$, and $\rho_f$ are porosity calculated by density log, bulk density from log, matrix density, and fluid density respectively.

The sonic porosity was calculated using the equation proposed by Wyllie (1963).

$$\emptyset_s= (\Delta T_{log}- \Delta T_{ma})/ (\Delta T_f- \Delta T_{ma}) \quad (5)$$

where $\emptyset_s$: is sonic-derived porosity, fraction; $\Delta t_{ma}$: is the matrix transit time [Its value is 47.6 μsec/ft for limestone and 43.5 μsec/ft for dolomite)]; $\Delta t_{log}$: is the interval transit time in the formation in μsec/ft; $\Delta t_f$ is identical to eq. 1.]. Sonic porosity versus Neutron-Density porosity cross plots were used to distinguish between intergranular vs. secondary porosity (equ. 6).

$$\emptyset_{ND}= [(\emptyset_D^2+ \emptyset_N^2)/2]^{1/2} \quad (6)$$

where $\emptyset_{ND}$ is Neutron-density porosity, $\emptyset_D$ is density porosity and $\emptyset_N$ is Neutron porosity. The total porosity is the average of density ($\emptyset_D$) and neutron ($\emptyset_N$) porosities:

$$\emptyset_T= (\emptyset_D + \emptyset_N)/2 \quad (7)$$

where core data are not available, the Archie constants could be calculated using well log data and Pickett cross-plot, (Asquith, and Gibson, 1983) and to calculate (*m* and a) from well logs (Morris and Biggs, 1967). The basis of this plot is the Archie's equation (Archie, 1942). By rearranging the equation, we will have:

$$S_w= I^{-1/n} \quad (8)$$

$$I= R_t/ R_0= R_t/ (FR_w) \quad (9)$$

$$F= a\emptyset_t^{-m} \quad (10)$$

By combining equations 8 and 10, equation 11 would be obtained:

$$R_t= a\emptyset_t^{-m} R_wI= a\emptyset_t^{-m} R_w S_w \quad (11)$$

By logarithm of equation 4, the following equation is obtained (Pickett, 1966):

$\log R_t = -m\log Ø_t + \log(aR_w) + \log I$ (12)

The intercept when PHI =1 is the value of $aR_w$ as shown in Fig. 8, and by knowing the value of Rw, the values of tortuosity factor (a) can be determined (El-Khadragy et al., 2014).

## Facies analysis and depositional environment

After examining thin sections prepared from cores and cutting chips, 9 microfacies were recognized in the Sarvak Formation (Table 1) which will be briefly introduced in the following section.

Barren mudstone/dolomudstone with rare (less than 5%) bioclasts. These beds were probably deposited on upper tidal flat to supratidal, where the stiff conditions prohibits any biota to survive. Bioclastic wackestone/packstone and peloid packstones associated by benthonic foraminifera (e. g. miliolids) and *Nezzazata* sp. and abundant peloids are indicative of a semi-restricted lagoon.

**Table 1.** Summary of facies analysis, interpretation and inferred depositional setting of the microfacies of the Sarvak Formation in the Marun oil filed

| Facies | Lithology, Texture | Grain size | Constituents | | Energy level | Depositional environment |
|---|---|---|---|---|---|---|
| | | | Skeletal | Non-skeletal | | |
| Sponge spicules planktonic fauna wackestone/ packstone | wackestone to packstone | Mud/ silt | Sponge spicules, Planktonic foraminifera (oligosteginids and *Hedbergella* sp.), calcisphere | - | Low | **Deep open-marine** |
| Planktonic foraminifera wackestone/ packstone | wackestone to packstone | Mud/ silt | Planktonic foraminifera (oligosteginids and *Hedbergella* sp.), calcisphere | - | Low | **Deep open-marine** |
| Bioclast- intraclast Oligosteginid packstone | packstone | Mud/sand | | Intraclast, peloid | Medium | **Shallow open-marine** |
| Rudist clasts benthic foraminifera floatstone/ wackestone | Limestone floatstone, | Sand-gravel | *Mangashtia* sp., *Orbitolina* sp. | Peloid | High | **Rudistic reef** |
| Coral boundstone/ floatstone | boundstone | Sand/ mud | Coral, green algae, *Nezzazata* sp., gastropod, *Alveolina* sp. and *Chrysalidina* sp., rudist and bivalve clasts | Peloid | High to medium | **Reef** |
| Ooid grainstone | grainstone | Sand | - | Ooid, peloid | High | **Shoal** |
| Peloid grainstone/ packstone | grainstone/ packstone | Sand | *Nezzazata* sp., miliolid, | Peloid, intraclast | Medium | **Lagoon** |
| Benthic foraminifera bioclast -peloid wackestone/ packstone | wackestone/ packstone | Sand | *Nezzazata* sp., miliolid, *Textularia* sp., gastropod, *Alveolina* sp., and *Chrysalidina* sp., rudist and bivalve debris | Peloid | Low | **Lagoon** |
| Mudstone | mudstone/ minor dolomudstones | Mud | Rare benthic foraminifera | | High to low | **Tidal flat** |

Ooid grainstone with less than 10% peloids may accumulated on shoals. Rudist floatstone and coral boundstones with large subrounded (comminuted) rudist clasts, echinoids, intraclasts and coral debris are frequent. These facies are presumably accumulated on the shelf margin and make rimmed shelfs. Boiclastic packstones with rudist and echinoderm clasts, peloids, oligoteginids and other planktonic foraminifera with lime mad matrix were possibly derived after erosion and reworking of the forereef facies of shelf edge into more quiet deep water. Mudstone/wackestone to packstones with small delicate planktonic foraminifers (i.e. *Hedbegella* sp., *Favosella* sp.), calcisphere, sponge spicules and abundant mud matrix are indicative of basinal facies. In brief, the Sarvak Formation was deposited a rimmed shelf with tidal flat, lagoon, shoals/bar, platform margin and basinal facies (Mohseni et al., 2015). They also introduced 4 3rd order depositional sequences in the Marun oil field.

## Results

### *Lithological and mineralogical interpretation*

Results for the Sarvak Formation (Figs. 3, 4, 5 and 6) show different lithology types. The rock types of the Upper Sarvak in the studied wells will be discussed as follow:

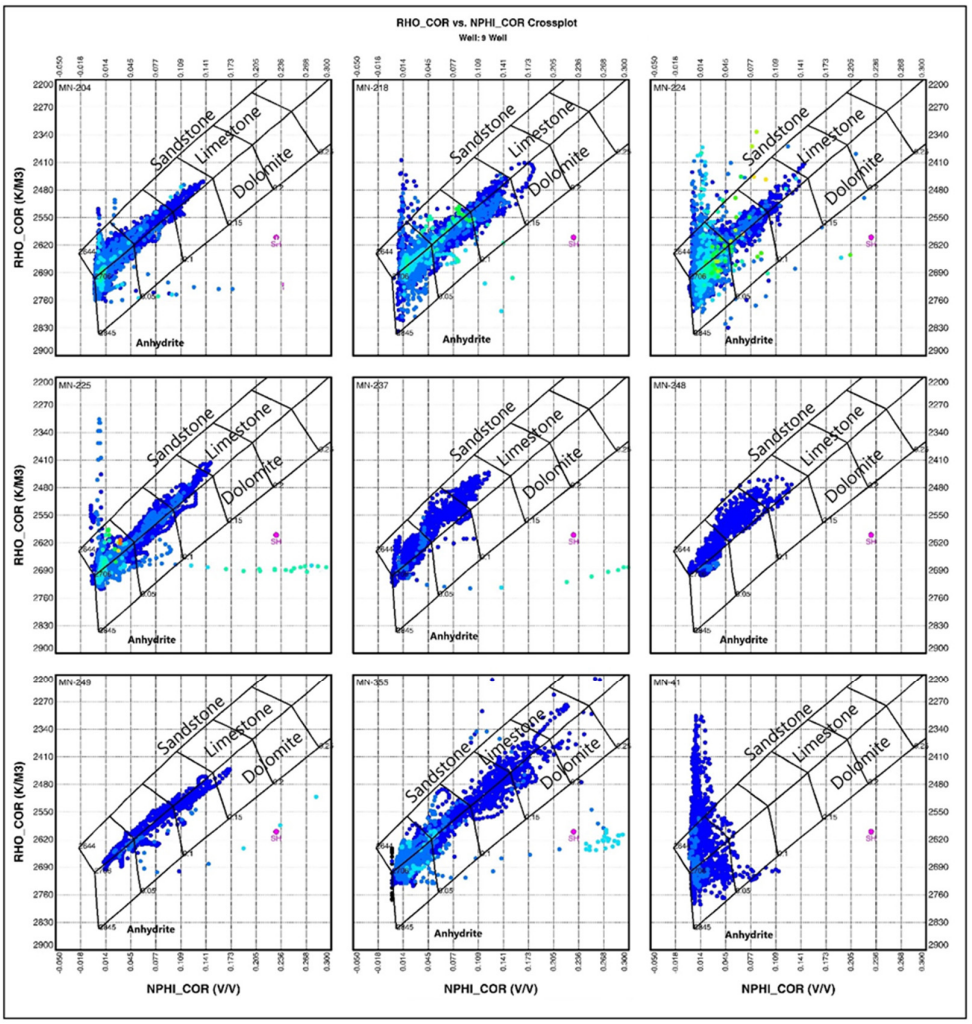


**Figure 3.** Neutron- Density cross-plots showing lithology categories of the Upper Sarvak reservoir in the selected borehole (Schlumberger, 1997)

Neutron (NPHI) versus Density (RHOB) cross-plot

Figure 3 illustrates the lithology and averaged porosity of the Sarvak reservoir obviously shows limestone lithology with a slight shift toward dolomite and shale.

Neutron (NPHI) versus sonic (DT) cross-plot

The results inferred from Fig. 4 are consistent with findings of Fig. 3 which indicate that lithology of the Sarvak Formation consists of limestone and dolomite and porosity types obtained from the other method.

M–N plot

In complex mineral mixtures, lithology interpretation is facilitated by using M-N plot (Serra, 2009). Since M and N are simply the slopes of the individual lithology lines on the sonic-density and density-neutron cross-plots, respectively; thus are essentially independent of porosity, and facilitates lithology identification (Schlumberger, 1998).

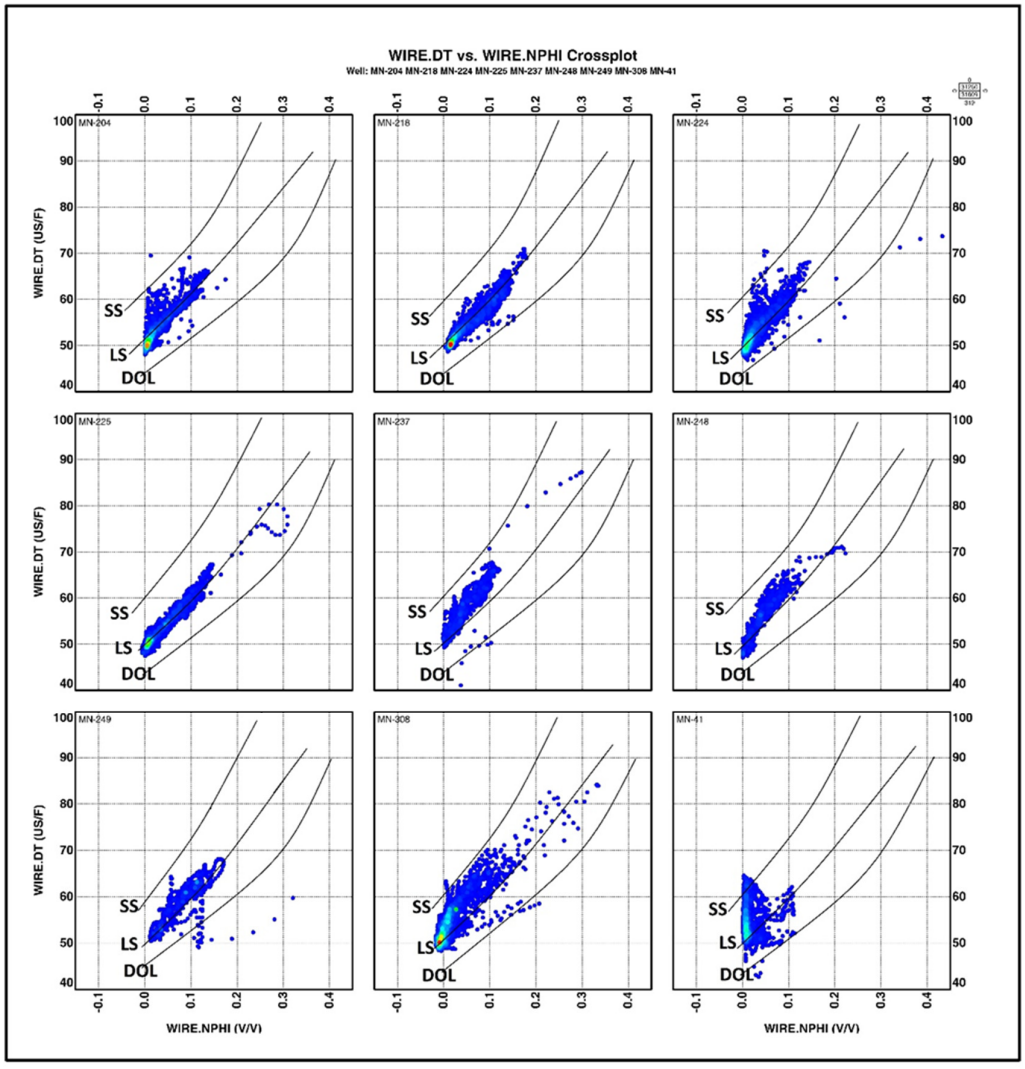


**Figure 4.** Neutron vs. sonic cross plot displaying the lithological composition of Upper Sarvak reservoir in some selected boreholes

These plots are illustrated in Fig. 5. Obviously, the Sarvak Formation consists of limestone (represented by calcite domain) with subordinate dolomite content.

However, some samples are located above the calcite and dolomite domains which could be due to so called gas effect. This is more pronounced in wells 218 and 224. Some samples shift somehow toward anhydrite domain (Fig. 5).

The Matrix Identification (MID) Plot

Lithology, gas, and secondary porosity determination can be obtained using the matrix identification (MID) plot. At first, the values of the apparent matrix density (ρma) and apparent matrix transit time (Δtma) must be obtained (Clavier and Rust, 1976).

The apparent matrix density values are about 2.7 to 2.87 gr/cm$^3$, and the amount of apparent matrix transit time is in the range of 45 to 55 μs/ft, which indicate limestone, dolomite and dolomitic limestone lithologies (Fig. 6).

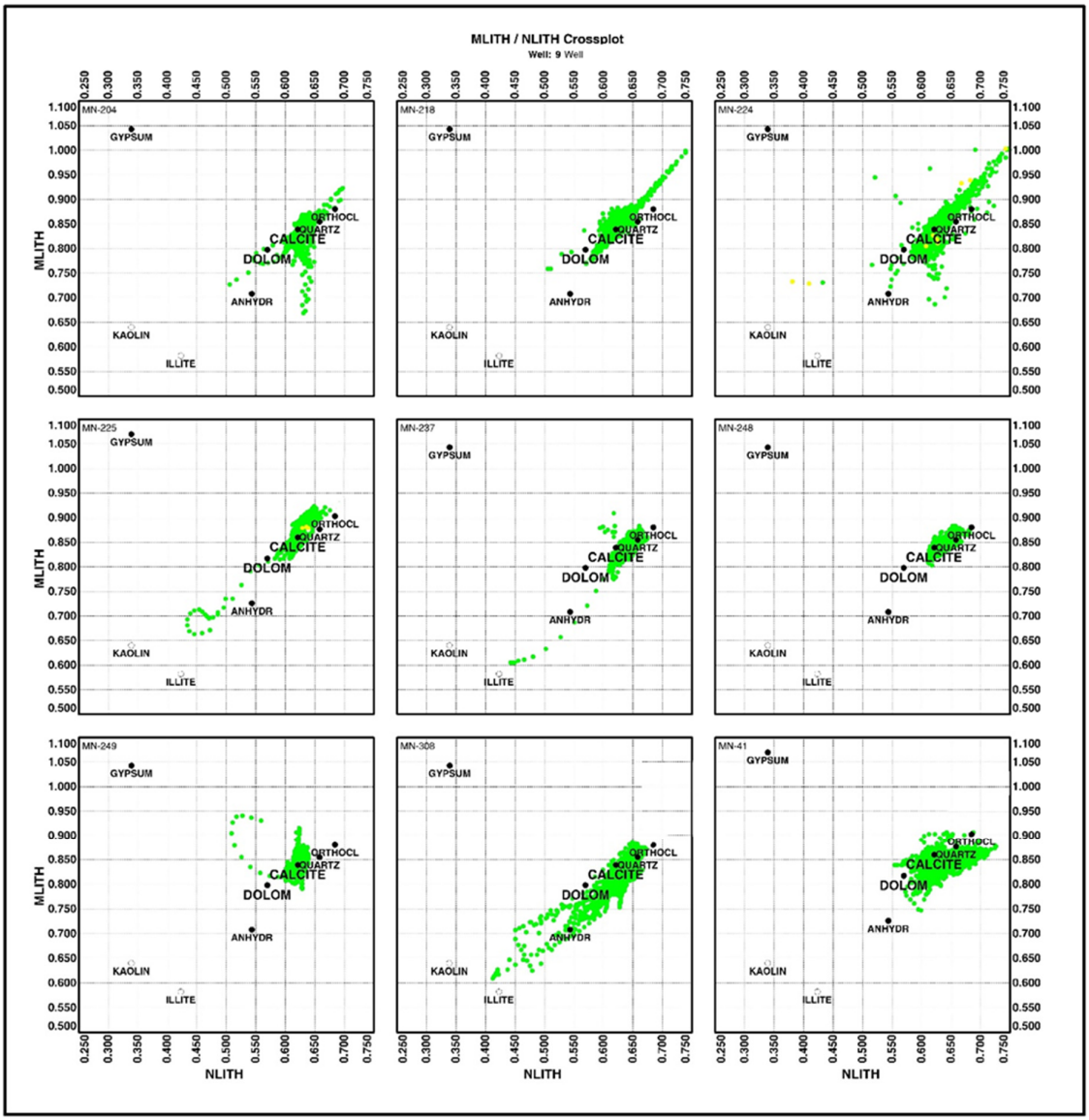


**Figure 5.** M-N plots showing lithological components of the Upper Sarvak reservoir in the selected wells

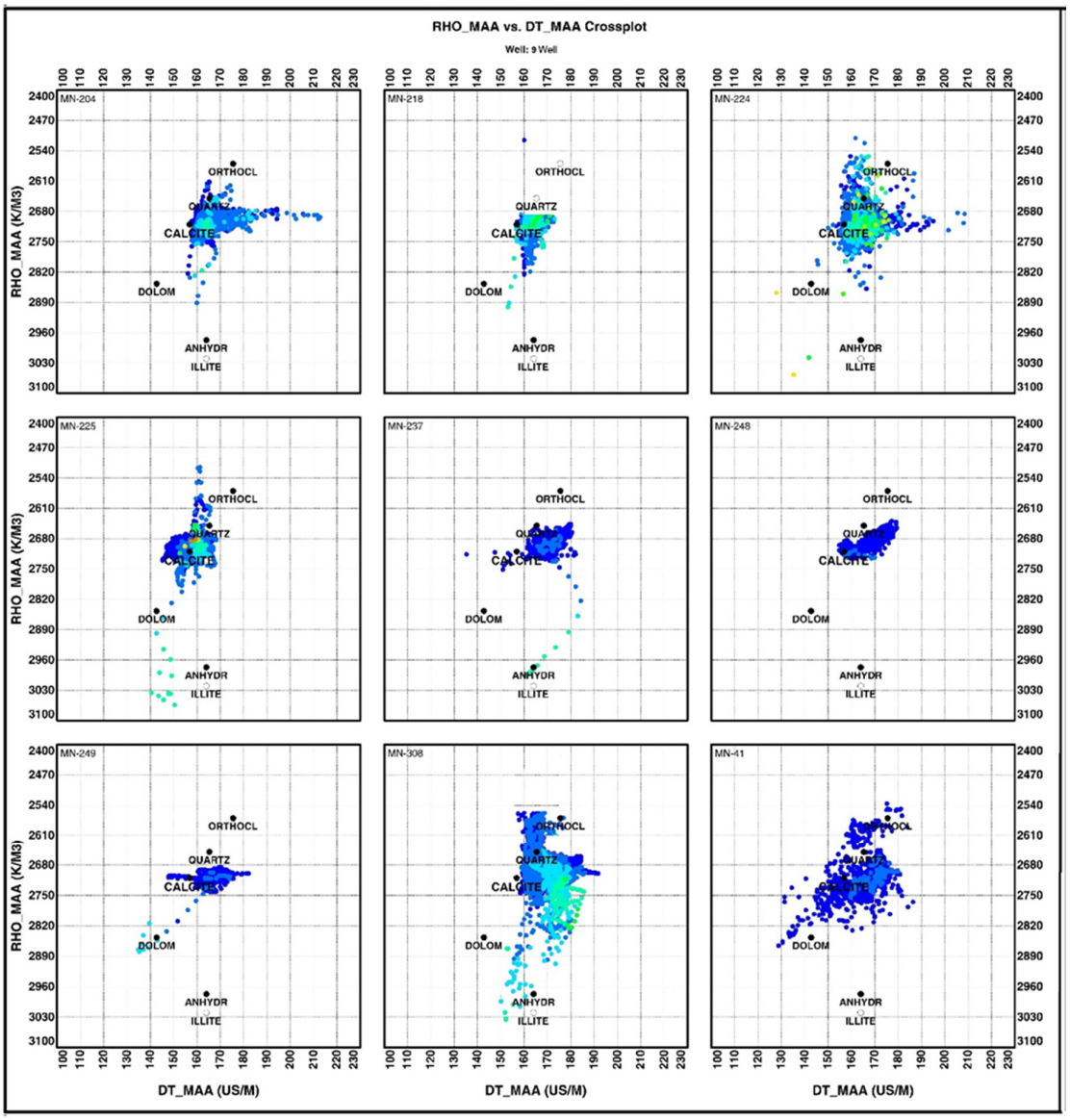


**Figure 6.** The Matrix Identification (MID) plots show lithology /mineralogical composition of the Upper Sarvak reservoir in the selected wells

*Petrophysical parameters*

This method was used to assess shale volume, porosity and water saturation, which were thereafter implemented to calculate hydrocarbon potential at the studied wells.

Shale volume

As indicated in Table 1, the average volume of shale is low, indicating a clean reservoir. A 50% cut off was also applied to differentiate between shaly and carbonate zones within the reservoir. The Vsh varies between 0.1 and 23.3%. The lowest shale volume was calculated for MN-308 and well# MN-224, while the highest value was observed in well# MN-204.

Log derived porosity

Porosity was calculated by using neutron and density logs, taking the bulk density reading

obtained from the formation density log and applying the Eq. (6).

The total porosity of the Upper Sarvak ranges from 0.8% to 47.2%, and effective porosity ranges from 0.1% to 45.1% (Table 1), the lowest value is in well# MN- 224 and the highest is in well# MN- 41. The type of porosity within the reservoir formation has been estimated by neutron-density log vs. sonic log cross plot (Fig. 8). This porosity is a combination of primary (intergranular) and secondary porosity. The presence of secondary pore type can be a result of partial or complete dissolution of carbonates during various diagenetic processes. The Upper Sarvak Formation could be considered as poor to good reservoir after (Levorson 1972) reservoir description scheme.

Fluid saturation

In clean and shale free reservoirs, water saturation is calculated by Archie method.

*Archie's parameters (m, n, and a)*

The Archie's parameters (m, n, and a) were determined using Pickett plot (Pickett, 1963, 1974,) (Fig. 9) which were used to calculate the water saturation that is reported in Table 2.

Results indicate that median water saturation (Sw) varies between 42% and 98.7%). Accordingly, the majority of this field show high and very high water saturation (excluding well# MN-249). The minimum value was calculated for well# MN-41 while the highest water saturation was observed in lower parts of all of the wells, possibly due to water flooding, consequently caused the lower part of the formation to be out of interest.

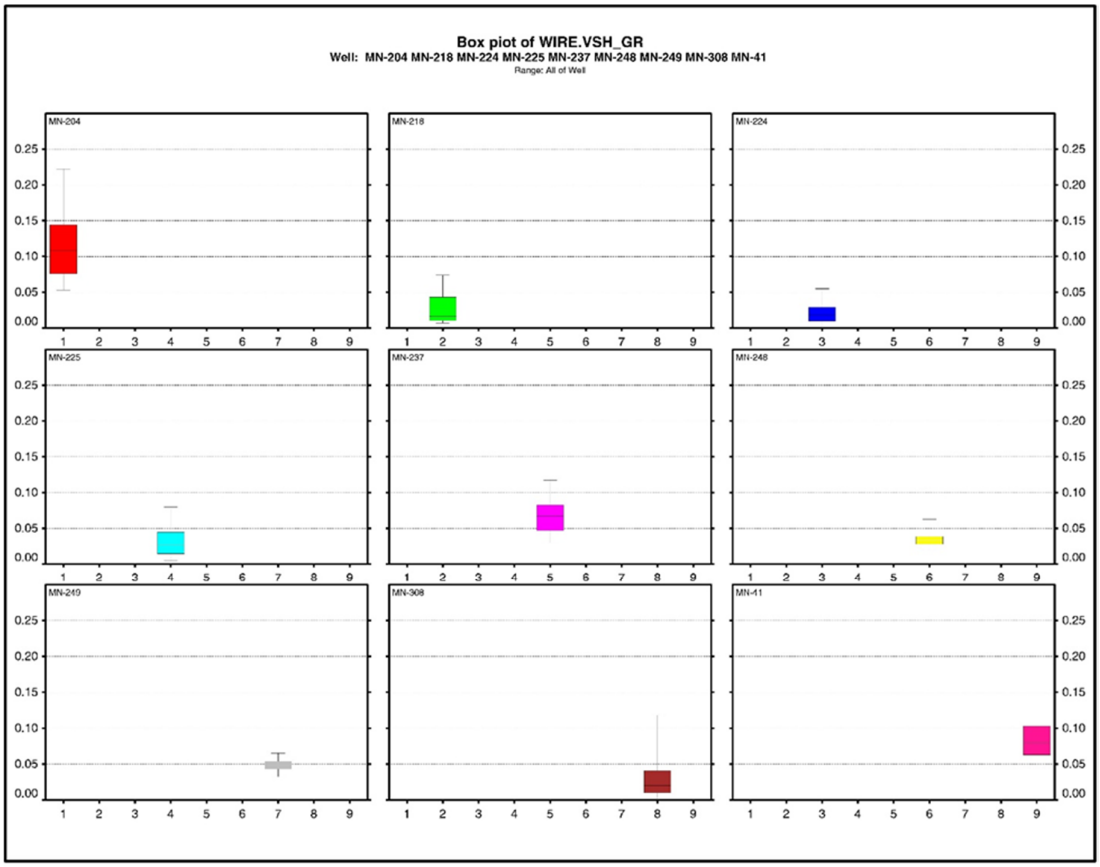


**Figure 7.** Boxplots showing shale volume of the Upper Sarvak reservoir in the studied wells

**Table 2.** The min. med. and max. of shale volume, total porosity, effective porosity and water saturation calculated in the Marun oil field

| Well | $V_{Sh}$ (%) | | | $PHI_T$ (%) | | | $PHI_E$ (%) | | | $S_W$ (%) | | |
|---|---|---|---|---|---|---|---|---|---|---|---|---|
| | Min | Med | Max | Min | Med | Max | Min | Med | Max | Min | Med | Max |
| MN-41 | 4.4 | 7.9 | 14.9 | 1.3 | 3.2 | 47.2 | 0.3 | 1.2 | 45.1 | 3.0 | 52.3 | 100 |
| MN- 204 | 5.2 | 10.9 | 22.3 | 1.3 | 3.0 | 9.1 | 0.4 | 1.4 | 7.2 | 18.4 | 98.7 | 100 |
| MN- 218 | 0.8 | 1.5 | 7.4 | 1.7 | 3.2 | 11.2 | 1.3 | 2.7 | 9.4 | 23.2 | 74.4 | 91.2 |
| MN- 224 | 0.1 | 1.8 | 5.8 | 0.8 | 2.1 | 8.2 | 0.1 | 1.7 | 8.0 | 20.6 | 97.7 | 100 |
| MN- 225 | 0.9 | 2.6 | 7.9 | 1.2 | 2.2 | 10.0 | 0.4 | 1.6 | 9.6 | 20.1 | 81.2 | 92.3 |
| MN-237 | 2.7 | 6.9 | 11.8 | 1.8 | 4.9 | 11.7 | 0.5 | 2.6 | 10.2 | 23.2 | 74.7 | 100 |
| MN- 308 | 0.1 | 1.2 | 12.0 | 1.0 | 2.1 | 8.0 | 0.2 | 1.1 | 7.3 | 8.3 | 92.1 | 100 |
| MN- 248 | 2.0 | 3.3 | 6.2 | 1.2 | 5.1 | 10.1 | 0.2 | 4.3 | 9.7 | 26.3 | 79.8 | 100 |
| MN- 249 | 2.8 | 4.8 | 6.6 | 2.2 | 8.4 | 12.3 | 1.3 | 7.9 | 11.7 | 21.4 | 42.2 | 100 |

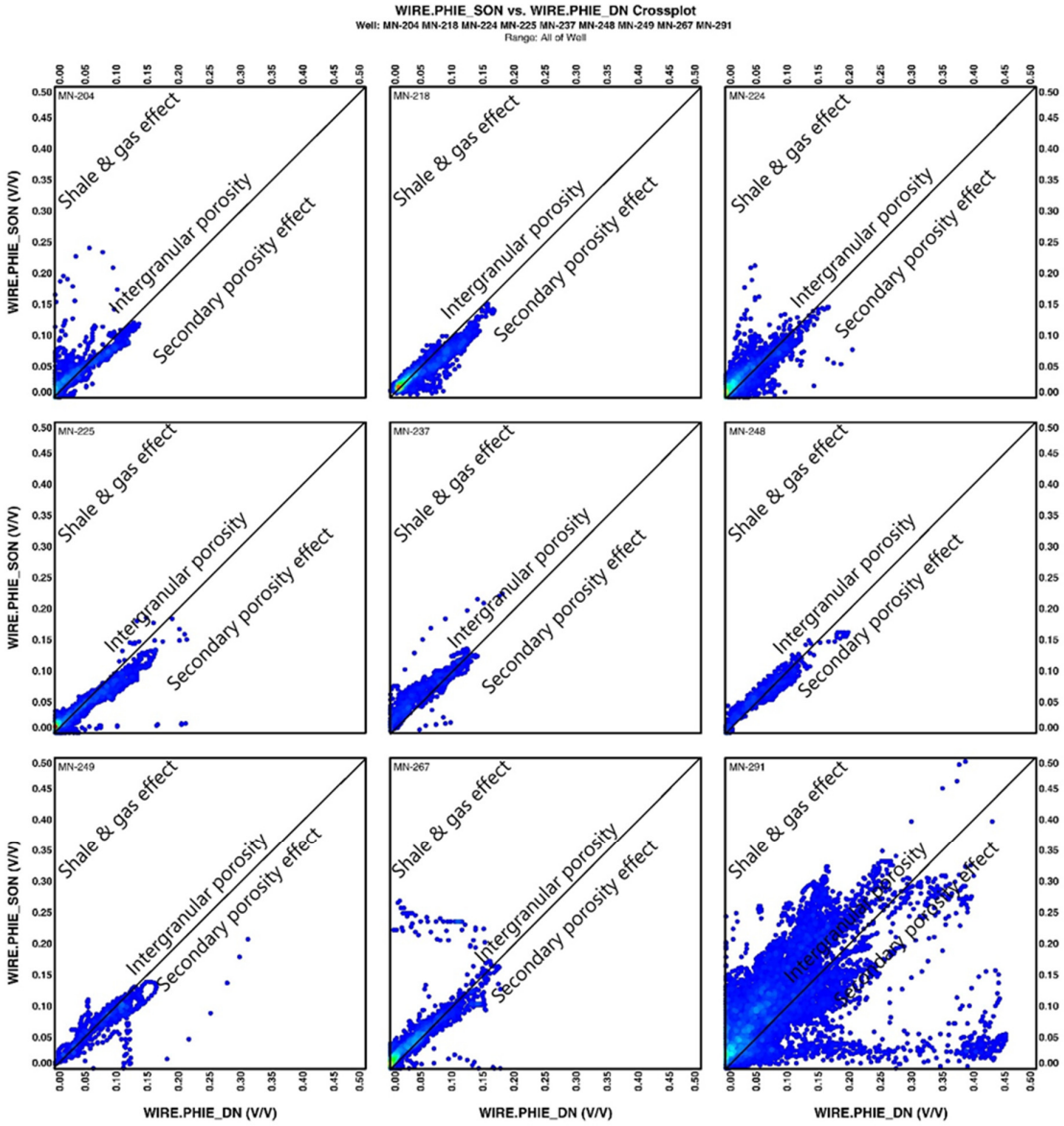


**Figure 8.** Cross-plots of porosity (neutron- density) vs. (sonic) showing porosity types in the Upper Sarvak reservoir in the selected wells

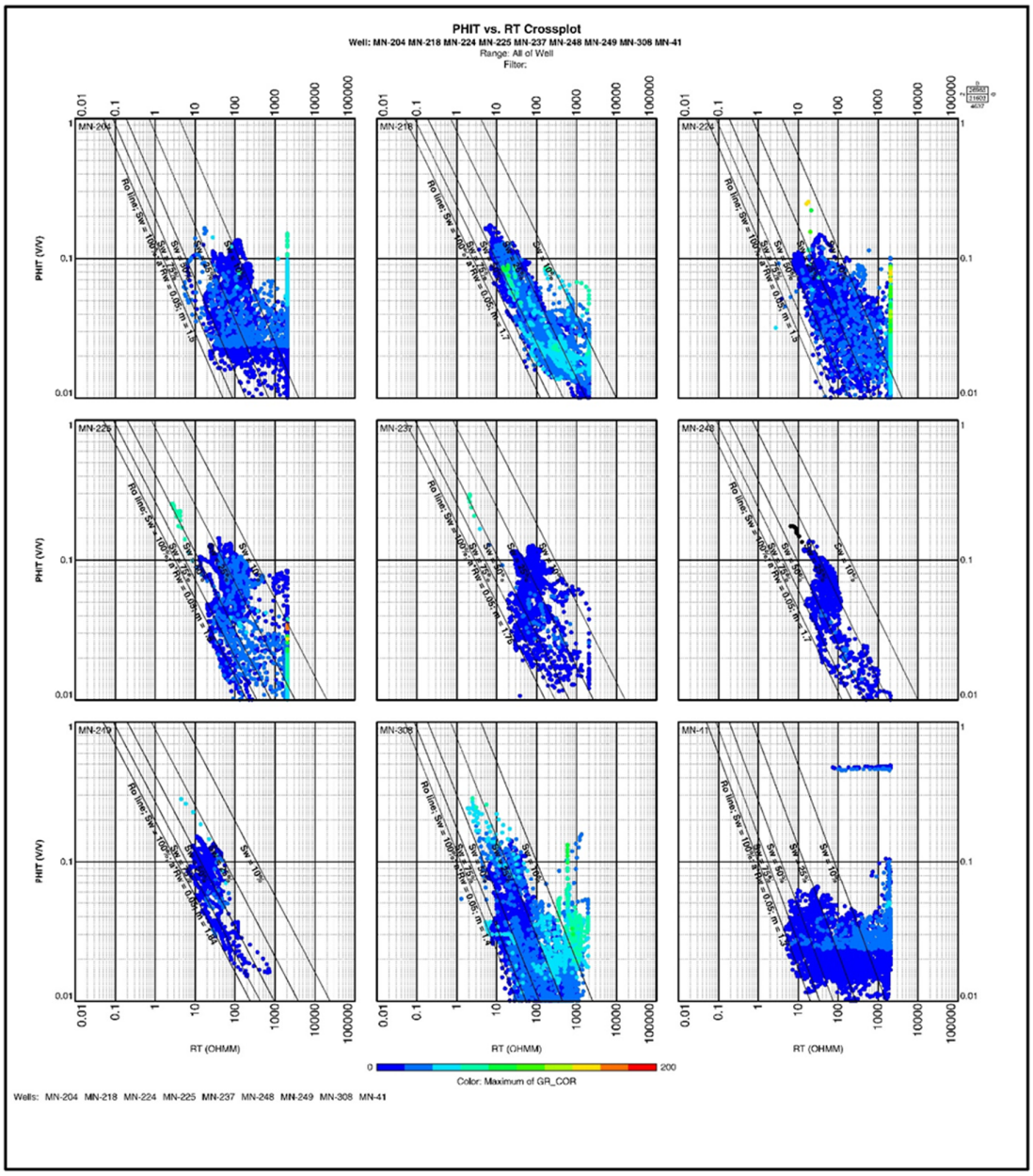


**Figure 9.** Pickett plot of porosity vs. resistivity (RT) in the Upper Sarvak

Figures 10 and 11 show examples for the implemented log data and some calculated petrophysical parameters for wells# MN-118 and MN-249.

## Discussion and inferred reservoir zoning

These calculations revealed that the upper part of the Sarvak formation comprises the most prolific and effective zone, which comprises the maximum porosity and hydrocarbon in place of the Marun oil field. Thus attempts were made to construct a 3-D model of effective porosity and water saturation in this field (Figs. 12 and 13). It is evident that majority of effective porosity are considerably concentrated in the middle part of this field (Fig. 12) which waning toward the both noses of the anticline (in SE and NW directions).

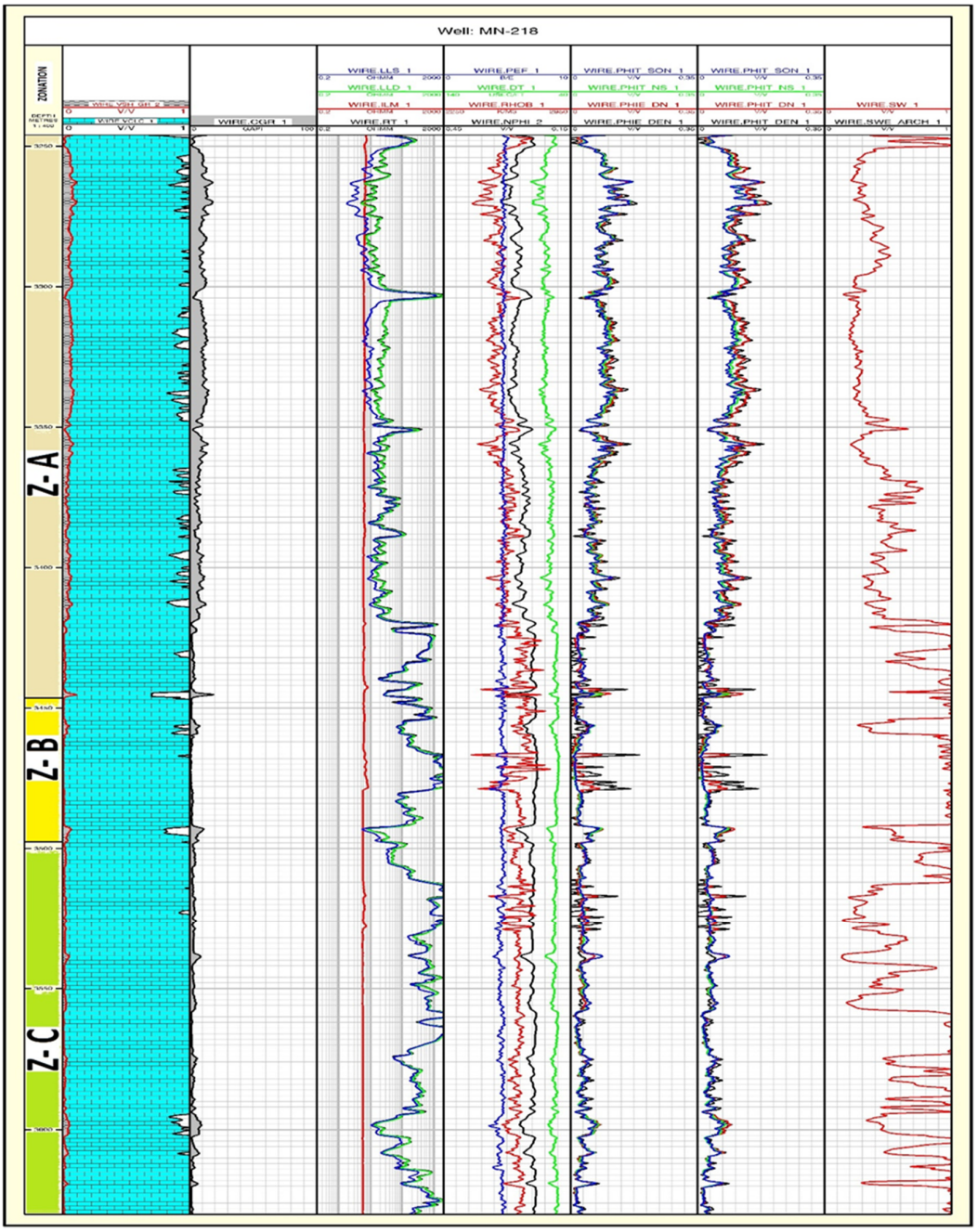


**Figure 10.** Various logs displaying variations in the petrophysical characteristics of the Upper Sarvak Formation in well# MN- 218

According to the 3-D model of water saturation (Fig. 13), seemingly $S_w$ increases toward the middle and east of the studied oil field. This in part could be controlled by extensive fractures which are concentrated in the middle part of the anticline (Qhanavati, 2000). Such extensional fractures are common in the outside of anticlines, while compressional fractures could normally develop inside of an anticline (Van Golf-Racht, 2010).

In terms of reservoir zoning, the Sarvak Formation could be divided into three major zones in the Marun oil field.

Zone A: Includes rock type IA/II of Archie's classification, comprising the topmost part of the formation is the best zone with high porosity, owing its reservoir quality to unconformity

related porosity-permeability development (*sensu* Rahimpor-Bonab et al., 2012); since it is in direct contact with the Cenomanian-Torunian unconformity on top. A significant sea-level fall coincided with the formation of the topmost part of the Sarvak Formation, consequently brought a type I sequence boundary which defines the upper contact with the Ilam Formation (Al-Sharhan and Nairn, 1990; Taghavi et al., 2006; Razin et al., 2010; Hajikazemi et al., 2010; Mohseni and Zeybaram Javanmard, 2020).

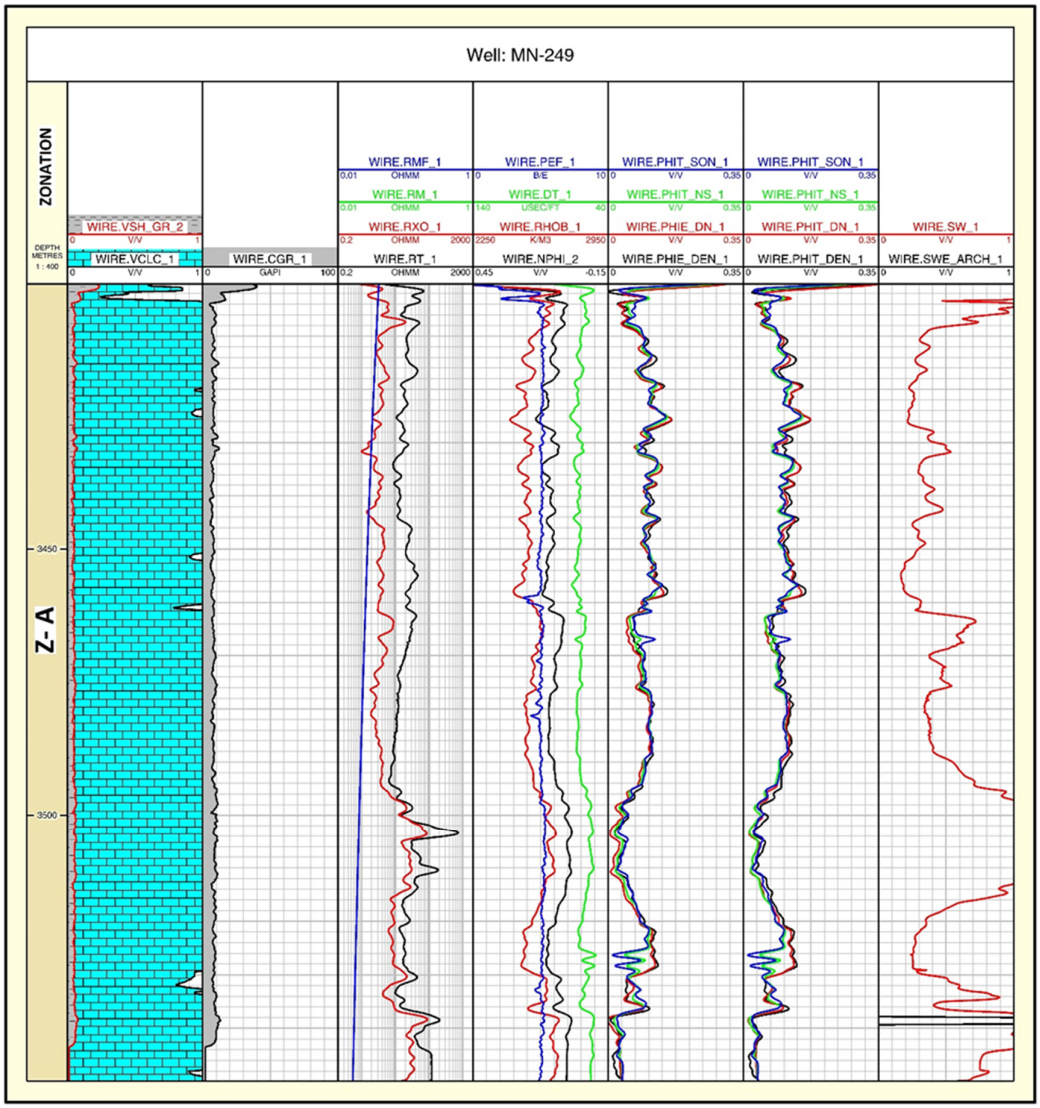


**Figure 11.** Various logs displaying variations in the petrophysical characteristics of the Upper Sarvak Formation in well# MN-249

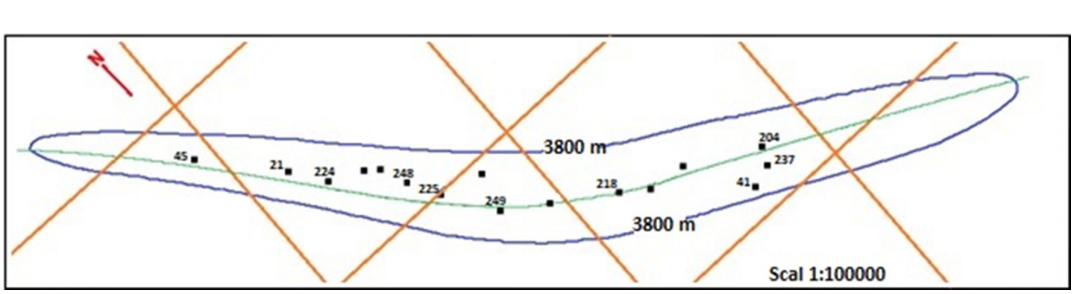


**Figure 12.** Location map of the studied wells on the structure contour map on top of the trap

**Table 3.** Average total porosity, water saturation and volume of shale for the Sarvak Formation in each zones

| Well No. | Top of zones (m) | | | Average porosity (%) | | | SW (%) | | | Average Shale volume (%) | | |
|---|---|---|---|---|---|---|---|---|---|---|---|---|
| | Z-A | Z-B | Z-C | Z-A | Z-B | Z-C | Z-A | Z-B | Z-C | Z-A | Z-B | Z-C |
| **MN-41** | 3616 | 3805 | 3850 | 9.1 | 1.2 | 5.7 | 33.4 | 0 | 21.5 | 10.9 | 7.6 | **12.4** |
| **MN-204** | 3267 | 3448 | 3499 | 8.4 | 2.4 | 5.4 | 21.1 | 17.9 | 36.2 | 9.6 | 7.7 | **13.2** |
| **MN-218** | 3246 | 3446 | 3498 | 10.0 | 2.5 | 6.4 | 32.0 | 33.9 | 34.6 | 3.4 | 2.3 | **4.6** |
| **MN-224** | 33401 | 3553 | 3622 | 7.7 | 1.11 | 6.1 | 24.2 | 37.5 | 16.0 | 3.1 | 2.7 | **4.1** |
| **MN-225** | 3395 | 3565 | 3650 | 8.8 | 5.9 | 7.71 | 19.5 | 16.9 | 28.5 | 3.2 | 2.6 | **4.4** |
| **MN-237** | 3368 | 3555 | N.P | 8.6 | 3.5 | - | 20.8 | 12.2 | - | 7.2 | 5.1 | **-** |
| **MN-248** | 3440 | 3610 | N.P | 7.8 | 0 | - | 30.7 | 0 | - | 4.6 | 3.9 | **-** |
| **MN-249** | 2410 | N.P | N.P | 10.7 | - | - | 31.8 | - | - | 4.9 | - | **-** |
| **MN-308** | 3320 | 3484 | 3537 | 5.3 | 1.3 | 3.4 | 27.1 | 8.3 | 21.2 | 3.2 | 2.8 | **5.1** |

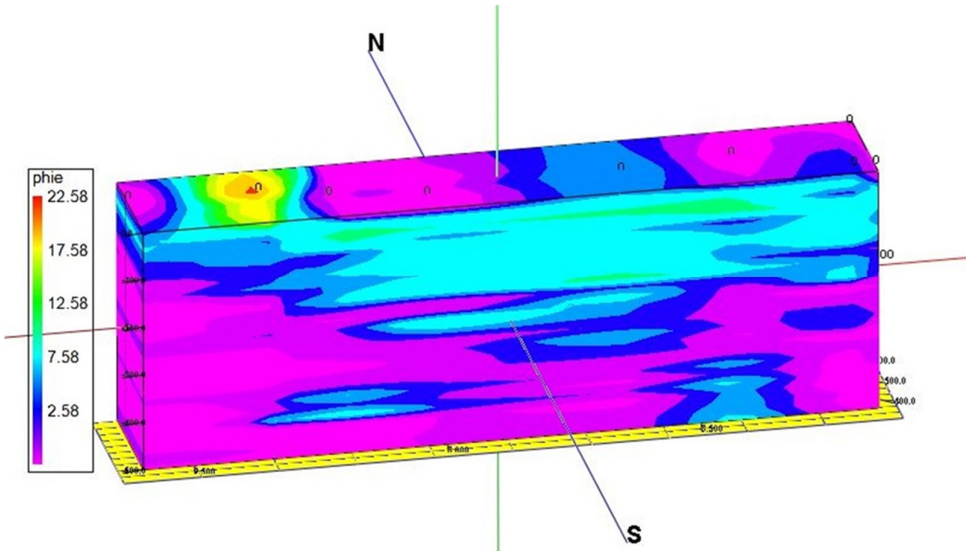


**Figure 13.** 3-D model of effective porosity distribution of Upper Sarvak Formation in the Maroon oil field

Local tectonic activities (basement faults movements) were invoked for this exhumation (Rahimpor-Bonab et al., 2010; Mehrabi et al., 2015; Asadi et al., 2016) despite global sea-level rise (Haq et al., 2014). Meteoric realm dissolution and karstification were frequently reported from this zone (Mohseni and Zeybaram Javanmard 2020 and references therein). From the central part of the anticline toward both flanks the thickness of zone A decreases down to 140m (Table 3). In the SE of this oil field (well# MN-41), the porosity of this zone drops to less 1%, while in contrast, the porosity increases westward (Table 3 and Fig. 13). Similar trend is true for the variations of water saturation and shale volume as well. Zone B: this zone is entirely composed of tight limestones with negligible porosity, hence acts a baffle zone (flow barrier) which separates the upper and lower flow units.

Zone C: this is composed of rock type IA to I/III of Archie's classification with recrystallized fine grain limestone intercalated with thin dolomitic beds. A minimum thickness was observed in the middle of the anticline (well# MN-225), while it becomes thicker west and eastward (Table 3). Average effective porosity of this zone is 6.2%, while it culminates to a maximum of 7.7% in well# MN-225), which is probably due to fracturing. Maximum water saturation of this zone is restricted to the middle part of the oil filed, which decreases toward the both plunges of the anticline (Table 3 and Fig. 14).

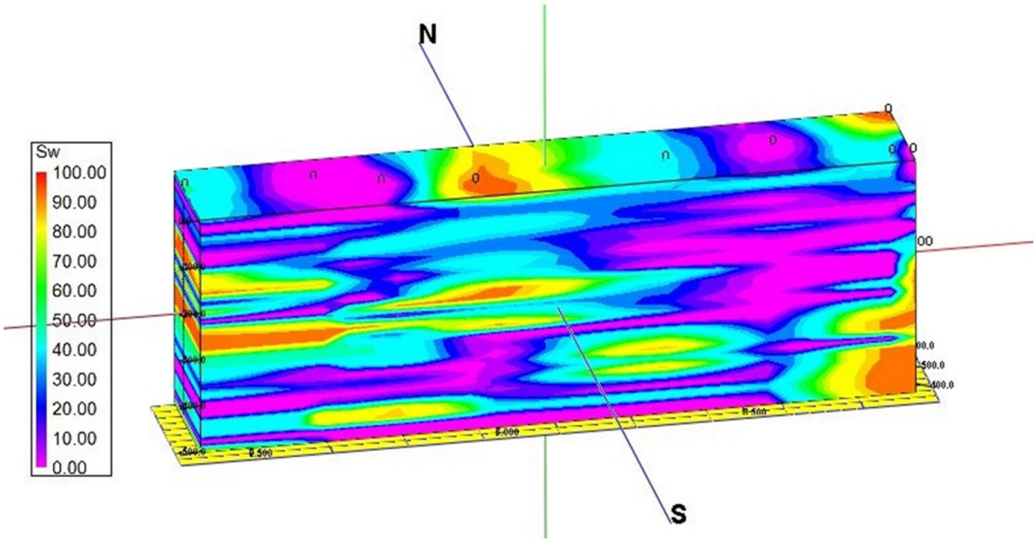


**Figure 14.** 3-D model of water saturation of Upper Sarvak Formation in the Maroon oil field

## Conclusions

Geological information and the results obtained from well log analysis in the Marun oilfield were used to study and evaluate the petrophysical characteristics of Mid Cretaceous Sarvak Formation. The present study provides an overview of the reservoir characteristics of this formation in the Marun oilfield.

The lithology and mineralogy of the Sarvak formation was identified based on the most suitable common methods. The Matrix Identification (MID), M-N plot and different cross-plots between porosity, NPHI- RHOB, NPHI- DT and indicated that the Sarvak Formation consists of carbonate (represented by calcite and dolomite domains) with few shale.

Average shale volume is low (mean 4.8%), so the Sarvak Formation could be considered as a clean reservoir.

Total, effective and secondary porosities were calculated. Intergranular and secondary porosities were observed within the Upper Sarvak Formation, which can play a vital role in emplacement of fluids within the reservoir. Secondary porosity indicates the effect of diagenesis and fracturing on the Sarvak Formation.

Water Saturation ranges from 3.0–100% and in the lower parts of the formation, influx of water made this zone out of economic interest.

Further study is recommended using core based petrophysical analysis. However, the present study is a pioneer in this types and can facilitate the understanding of the reservoir characteristics of the Sarvak Formation in the Marun oilfield.

## Acknowledgement

Part of this study was funded by a grant to H. Mohseni, from Vice-President Research Affair of Bu Ali Sina University. The authors also would like to extend their thanks to the Department of Developing Geology, National Iranian South Oil Co. (NISOC), for providing the data set. Our thanks are also due to the reviewers of *Geopersia*, who's critical review and constructive comments improved the quality of the manuscript both editorially and scientifically.

## References

Abd El-Gawad, E.A., 2007. The use of well logs to determine the reservoir characteristics of Miocene

rocks at the Bahar North East field, Gulf of Sues. Egyptian Journal of Petroleum, 30 (2): 175-188.
Al Sharhan, A.S. and Narin, A.E.M., 2003. Sedimentary basin and petroleum geology of the Middle East, Amsterdam, The Netherlands, Elsevier Science B. V., 979 pp.
Alavi, M., 2004. Regional stratigraphy of the Zagros fold-thrust belt of Iran and its pro-foreland evolution. Am J. Sci. 304:1-20.
Alsharhan, A.S., Nairn, A.E.M., 1990, A review of the Cretaceous formations in the Arabian Peninsula and Gulf: Part III. Upper Cretaceous (Arume group) stratigraphy and paleogeography: Journal of Petroleum Geology, 13 (3): 247- 266.
Archie, G.E., 1942. The electrical resistivity logs as an aid in determining some reservoir characteristics, Trans. AIME 146: 54-67.
Asquith, G.B., Gibson, C.R., 1983. Basic Well Log Analysis for Geologists. Methods in Exploration Series, 2end print (revised), AAPG, Tulsa, Oklahoma USA. 218 pp.
Assadi, A., Honarmand, J., Moallemi, S. A., Abdollahie‐Fard, I., 2016. Depositional environments and sequence stratigraphy of the Sarvak Formation in an oil field in the Abadan Plain, SW Iran. Facies 62: 26. DOI: 10.1007/s10347-016-0477-5.
Beiranvand, B., Ahmadi, A. and Sharafodin, M., 2007. Mapping and classifying flow units in the upper part of the mid-Cretaceous Sarvak formation (Western Dezful Embayment, SW Iran) based on a determination of the reservoir types. Jour. Petrol. Geol. 30: 357-373.
Bordenave, M.L., Hegre, J.A., 2010. Current distribution of oil and gas fields in the Zagros Fold Belt of Iran and contiguous offshore as the result of the petroleum systems. Geological Society, London, Special Publications, 330 (1): 291-353.
Casini, G., P.A., Gillespie, P.A., Vergés, J., Romaire, I., Fernández, N., Casciello, E., Saura, E., Mehl, C., Homke, S., Embry, J.C., Aghajari, L., and Hunt, D.W., 2011. Sub-seismic fractures in foreland fold and thrust belts: insight from the Lurestan Province, Zagros Mountains, Iran. Petroleum Geoscience, 17: 263-282.
Clavier, C., and Rust, D.H., 1976, MID Plot: A new lithology technique, Log analyst, 17 (6): 16.
El-Khadragy, A. A., Ghorab, M. A., Shazly, T.F., Ramadan, M., El-Sawy, M. Z., 2014. Using of Pickett's plot in determining the reservoir characteristics in Abu Roash Formation, El-Razzak Oil Field, North Western Desert, Egypt. Egyptian Journal of Petroleum, 23: 45-51.
Ellis, D.V., Singer, J.M., 2008. Well Logging for Earth Scientists, 2nd Edition, Springer Science and Business Media B.V. 699pp.
Ghabeishavi, A., Vaziri-Moghaddam, H., Taheri, A., Taati, F., 2010. Microfacies and depositional environment of the Cenomanian of the Bangestan anticline, SW Iran. J. Asian Earth Sci. 37: 275 - 285.
Hajikazemi, E.; Al-Aasm, I.S.; Coniglio, M., 2010. Subaerial exposure and meteoric diagenesis of the Cenomanian-Turonian Upper Sarvak Formation, southwestern Iran, Geological Society London Special Publications 330 (1): 253-272.
Haldorsen, H.H., Damsleth, E., 1993. Challenges in reservoir characterization. The American Association of Petroleum Geologists Bulletin, 77 (4): 541-551.
Hollis, C., 2011. Diagenetic controls on reservoir properties of carbonate successions within the Albian-Turonian of the Arabian Plate. Pet. Geosci. 17: 223-241.
James, G., Wynd, J.G., 1965. Stratigraphic nomenclature of the Iranian oil consortium agreement area. AAPG (Am. Assoc. Pet. Geol.) Bull. 49: 2182-2245.
Kumar, M., Dasgupta, R., Singha, D, K., Singh, N. P., 2017. Petrophysical evaluation of well log data and rock physics modeling for characterization of Eocene reservoir in Chandmari oil field of Assam-Arakan basin, India, Journal of Petroleum Exploration and Production Technology, 8 (2): 323- 340.
Lapponi, F., Casini, G., Sharp, I., Blendinger, W., Fernández, N., Romaire, I., and Hunt, D., 2011. From outcrop to 3D modelling: a case study of a dolomitized carbonate reservoir, Zagros Mountains, Iran. Petroleum Geoscience, 17: 283-307.
Mehrabi, H., Rahimpour‐Bonab, H., Hajikazemi, E., Jamalian, A., 2015. Controls on depositional facies in Upper Cretaceous carbonate reservoirs in the Zagros area and the Persian Gulf, Iran. Facies 61 (4): 1-24.
Mohseni, H.; Habibi asl, E., Ghanavati, K., 2015. Microfacies, depositional environment, sequence stratigraphy and diagenetic processes of the Sarvak Formation in the Marun oil field, Stratigraphy and Sedimentology Research, 31 (2): 51-66 (in Persian with abstract in English).

Mohseni, H., Zeybaram Javanmard, R. 2020. New data on sequence stratigraphy of the Sarvak Formation in Malekshahi city, (Ilam province) Zagros basin, Iran, Marine and Petroleum Geology, 112: https://doi.org/10.1016/j.marpetgeo.2019.104035.

Moradi, M., Tokhmechi, B., Masoudi, P., 2019. Inversion of well logs into rock types, lithofacies and environmental facies, using pattern recognition, a case study of carbonate Sarvak Formation. Carbonates and Evaporites, 34: 335-347.

Morris, R. L., and Biggs, W. P., 1967. Using log-derived values of water saturation and porosity" in 8th Annual Logging Symposium, (Society of Petrophysics and Well Log Analysts, Denver, Colorado, 1-26.

Mostafa, H.K., Walid, H.M., 2003. Estimation of shale volume using a combination of the three porosity logs. Journal of Petroleum Science and Engineering, 40: 145-157.

Motiei, H., 1995. Petroleum geology of Zagros. Geological Survey of Iran, Treatise on the Geology of Iran. Geological Survey of Iran, Tehran. (Two vol. in Persian), 1009 pp.

Pickett, G. R., 1972. Practical formation evaluation: Golden Colorado, G. R. Pickett, Inc.

Pickett, G. R., 1966. A review of current techniques for determination of water saturation from log, J. Petrol. Technol. 18: 1425-1433.

Qhanavati, K., 2000. NISOC unpublished open file No. 4946.

Rahimpour-Bonab, H., H. Mehrabi, A. H. Enayati-Bidgoli, M. Omidvar, 2012, Coupled imprints of tropical climate and recurring emergence on reservoir evolution of a mid-Cretaceous carbonate ramp, Zagros Basin, Southwest Iran: Cretaceous Research, 37: 15-34.

Rahimpour-Bonab, H., Mehrabi, H., Navidtalab, A., Omidvar, M., Enayati-Bidgoli, A. H., Sonei, R., Sajjadi, F., Amiri-Bakhtyar, H., Arzani, N. and Izadi-Mazidi, E., 2013. Palaeoexposure surfaces in Cenomanian-Santonian carbonate reservoirs in the Dezful Embayment, SW Iran. Journal of Petroleum Geology, 36(4): 335 - 362.

Razin, P., Taati, F., Van Buchem, F.S.P., 2010. Sequence stratigraphy of cenomanian- turonian carbonate platform margins (Sarvak formation) in the high Zagros, SW Iran: an outcrop reference model for the Arabian plate. In: In: Van Buchem, F.S.P., Gerdes, K.D., Esteban, M. (Eds.), Mesozoic and Cenozoic Carbonate Systems of the Mediterranean and the Middle East Stratigraphic and Diagenetic Reference Models, vol. 329. Geological Society, London, Special Publications, 187-218.

Rider, M. H., 2002. The Geological Interpretation of Well Logs, John Wiley and Sons, New York.

Sarasty, J. J., Stewart, R. R., 2003. Analysis of well-log data from the White Rose oilfield, offshore Newfoundland. CREWES Res Rep 15:1-16.

Schlumberger, 1991. Schlumberger Log Interpretation Principles/Application. Schlumberger Ed. Serv.

Schlumberger, 1997. Log Interpretation Charts, Schlumberger Wireline and Testing, Houston, Texas.

Schlumberger, 2009. Log Interpretation Charts, Schlumberger Well Services, Houston, 310 pp.

Schlumberger, Log Interpretation Manual/Applications‖, 1974. Houston, Schlumberger Well Service, Inc. 2, 1l6 pp.

Schlumberger. 1998. Cased Hole Log Interpretation Principles/Applications. Houston, Schlumberger Wireline and Testing.

Selley, R. C., 1998, Elements of Petroleum Geology, Academic Press, USA, 2nd ed., 470 pp.

Sepehr, M., Cosgrove, J., 2004. Structural framework of the Zagros fold-thrust belt, Iran. Mar. Pet. Geol. 21: 829-843.

Serra, O., 2009, Fundamentals of well-log interpretation, University of Paris, 487 pp.

Setudehnia, A., 1978. The Mesozoic sequence in southwest Iran and adjacent areas. J. Pet. Geol. 1,: 3-42.

Sharma, M., Hemant Singh, K., Pandit, S., Kumar, A., and Soni, A., 2020, Petrophysical Modelling of Carbonate Reservoir from Bombay Offshore Basin. In: Hemant Singh, K., Mohan Joshi, R., (eds.), Petrophysics and rock physics of carbonate reservoirs. Springer Nature Singapore Pte Ltd. 299 p.

Sharp, I., Gillespie, P., Morsalnezhad, D., Taberner, C., Karpuz, R., Verge's, J., Horbury, A., Pickard, N., Garland, J., Hunt, D., 2010. Stratigraphic architecture and fracture controlled dolomitization of the Cretaceous Khami and Bangestan groups: an outcrop case study, Zagros Mountains, Iran. In: In: van Buchem, F.S.P., Gerdes, K.D., Esteban, M. (Eds.), Mesozoic and Cenozoic Carbonate Systems of the Mediterranean and the Middle East: Stratigraphic and Diagenetic Reference Models, vol. 329. Geological Society, London, Special Publications, 343-396.

Taghavi, A.A., Mørk, A., Emadi, M.A., 2006. Sequence stratigraphically controlled diagenesis governs

the reservoir quality of a carbonate reservoir from southwest Iran. Pet. Geosci. 12: 115-126.
Taghavi, A.A., Mørk, A., Kazemzadeh, E., 2007. Flow unit classification for geological modelling of a heterogeneous carbonate reservoir: cretaceous Sarvak Formation, Dehluran Field, SW Iran. J. Pet. Geol. 12: 115-126.
Tiab, D., 2000. Advances in petrophysics, University of Oklahoma, 129- 169.
Van Buchem, F.S.P., Razin, P., Homewood, P.W., Oterdoom, W.H., Philip, J., 2002. Stratigraphic organization of carbonate ramps and organic rich intrashelf basins: Natih Formation (middle Cretaceous) of northern Oman. Am. Assoc. Pet. Geol. Bulletin 86: 21-53.
Van Buchem, F.S.P., Simmons, M., Droste, H., Davies, R., 2011. Late Aptian to Turonian stratigraphy of the eastern Arabian Plate-depositional sequences and lithostratigraphic nomenclature. Pet. Geosci. 17: 211-222.
Van Golf-Racht, T.D., 1982. Fundamentals of fractures reservoir engineering, Elsevier Science, 732 pp.
Vincent, B., Van Buchem, F.S.P., Bulot, L., Jalali, M., Swennen, R., Hosseini, A., Baghbani, D., 2015. Depositional sequences, diagenesis and structural control of the Albian to Turonian carbonate platform systems in coastal Fars (SW Iran). Mar. Pet. Geol. 63: 46-67.
Wu, W., Grana, D., 2017. Integrated petrophysics and rock physics modeling for well log interpretation of elastic, electrical, and petrophysical properties. Journal of Applied Geophysics 146: 54-66.
Wyllie, M.R.J., 1963. The fundamentals of well log interpretations. Academic Press, New York, 238 p.
Ziegler, M., 2001. Late Permian to Holocene paleofacies evolution of the Arabian plate and its hydrocarbon occurrences. GeoArabia 6: 445-504.
Wyllie, M., Gregory, A., and Gardner, L. (1956) Elastic wave velocities in heterogeneous and porous media. Geophysics, 21: 41-70